IEEE Access
Multidisciplinary | Rapid Review | Open Access Journal

Received June 30, 2020, accepted July 6, 2020, date of publication July 16, 2020, date of current version July 28, 2020.

Digital Object Identifier 10.1109/ACCESS.2020.3009738

Autonomous Wind-Turbine Blade Inspection Using LiDAR-Equipped Unmanned Aerial Vehicle

MARKO CAR, (Member, IEEE), LOVRO MARKOVIC, (Member, IEEE), ANTUN IVANOVIC, (Member, IEEE), MATKO ORSAG, (Member, IEEE), AND STJEPAN BOGDAN, (Senior Member, IEEE)

Faculty of Electrical Engineering and Computing, University of Zagreb, 10000 Zagreb, Croatia

Corresponding author: Marko Car (marko.car@fer.hr)

This work was supported by the European Commission Horizon 2020 Programme through the Project Twinning Coordination Action for Spreading Excellence in Aerial Robotics (AeRoTwin) under Grant 810321 and through the Project ENergy aware BIM Cloud Platform in a COst-effective Building REnovation Context (ENCORE) under Grant 820434. Furthermore, this research was a part of the scientific project Autonomous System for Assessment and Prediction of infrastructure integrity (ASAP) financed by the European Union through the European Regional Development Fund-The Competitiveness and Cohesion Operational Programme (KK.01.1.1.04.0041).

ABSTRACT This paper presents a LiDAR-equipped unmanned aerial vehicle (UAV) performing semi-autonomous wind-turbine blade inspection which includes traversing to the blade tip and back, while keeping constant relative distance and heading to the blade plane. Plane detection is performed applying the RANSAC method on a subset of the gathered pointcloud. Utilizing the relative distance to the inferred plane as well as its normal vector, the UAV is able to maintain a constant distance and heading towards the plane while moving in parallel with it. The proposed procedure performs successful wind-turbine blade inspections with minimal operator involvement. Inspection results include high-resolution blade images as well as a 3D model of the wind-turbine structure. Finally, to show the feasibility of this approach, simulations are performed on a wind-turbine model and experimental results are presented for an outdoor single-blade inspection scenario both on a mock-up setup and a full-scale wind-turbine blade. It is worth noting that the system's adequacy has been fully validated in real conditions on an operational wind farm.

INDEX TERMS Control systems, inspection, robotics and automation, unmanned aerial vehicles, wind farms.

I. INTRODUCTION

Interest in UAVs, both scientific and industrial, has grown considerably over the years. As they have gained in autonomy, their range of applications has significantly widened. Endowed with various sensor suites, tasks such as surveillance, inspection [3]–[5], search and rescue [6], 3D mapping [7], etc. are well within their operational reach. Light detection and ranging (LiDAR) sensors are particularly interesting for their ability to collect large number of accurate point coordinates at long range. Pairing them with UAVs makes a potent combination for tackling more complex tasks. The main goal of this paper is to present the application of a LiDAR-equipped UAV in a wind-turbine blade inspection scenario.

Modern wind-turbine farms are often placed in remote locations with featureless surroundings. During their active periods, wind-turbines are likely to suffer structural damage. For maximum operational efficiency incurred damage should be timely managed which warrants frequent inspections. Manually operated UAVs are not a novelty in this area as their use is convenient in adverse, high-altitude environments. Companies such as *Helvetis* are already successfully performing manual UAV wind-turbine blade inspections both on-land and off-shore providing high-resolution blade images. However, manual inspections usually require at least two people present at the site, one being a skilled pilot while the other an on-board camera operator. Keeping the camera in focus during the whole inspection process implies holding a constant relative distance from the blade which often proves difficult during high-altitude, windy conditions. For practical and research purposes, automating this process seems an obvious way forward.

Previous research regarding wind-turbine inspection methods in [8] applies a Cooperative Coverage Path Planning (C-CPP) algorithm for a wind-turbine inspection task. Multiple LiDAR-equipped UAVs are given predefined, offline-generated trajectories, during which relevant data

The associate editor coordinating the review of this manuscript and approving it for publication was Yang Tang.

FIGURE 1. Custom built UAV equipped with a Velodyne VLP-16 LiDAR sensor filmed mid-flight while performing a manually operated inspection procedure on a wind-turbine blade.

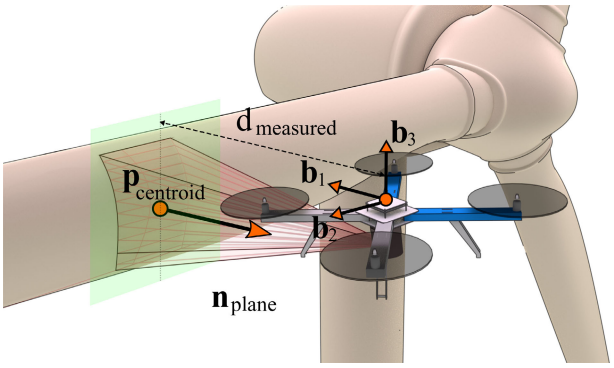

FIGURE 2. This figure shows a LiDAR equipped UAV performing an autonomous wind-turbine blade inspection. Through the obtained point cloud analysis the UAV is able to keep constant relative distance $d_{measured}$ while keeping heading parallel with the plane normal vector n_{plane}. Lastly, vertical offset from $p_{centroid}$ vector is used for maintaining UAV altitude at the center of the blade at all times.

is collected for post-processing and 3D model building. Similar work includes [9] where a mathematical wind-turbine model is obtained through offline video processing of a given wind-turbine structure. After extracting position reference points from the mathematical model, the UAV executes a generated trajectory during the inspection process. Furthermore, in [10] machine vision algorithms are used on the visual sensor data to perform online localization of the UAV w.r.t. the wind-turbine rotor.

On the other hand, the work done in this paper aims to demonstrate execution of LiDAR-based, online generated UAV reference points along the wind-turbine blade. Although a pilot is required to position the UAV against the wind-turbine blade, after initiating the inspection procedure the UAV will autonomously move to the blade tip and back while keeping constant relative distance and perpendicular heading. A LiDAR sensor is essential for this task as it enables the inspection to be performed in off-shore environments and to obtain a 3D model of the wind-turbine structure. A Velodyne VLP-16 LiDAR is chosen for this task as the need for reliable, high precision measurements which feed back to the inspection controller heavily outweigh the steep cost of the sensor. Considering the fact that the aim for this system is a fully autonomous inspection performed on valuable target structures such as wind-turbines, the sensor cost is justifiable in the big picture. An in-depth analysis of VLP-16 measurement uncertainty and mathematical model is shown in [11]. Use of stereo-cameras was considered, though dismissed, as their performance is inadequate in featureless surroundings. The quality of image-only inspections is often affected by motion blur as presented in [12].

The proposed inspection method relies on extracting current wind-turbine blade information such as relative distance to the blade along with its normal vector as seen in Fig. 2. Random sample consensus (RANSAC) algorithm is applied to a segment of the collected point cloud data in order to extract plane parameters.

Previous research conducting surface estimation and detection experiments using 3D LiDAR include [13], [14] where authors presented road surface detection results using principal component analysis (PCA) and a general ground plane detection using RANSAC respectively. A SLAM based approach in [15] presents a point cloud segmentation method wrt. the corresponding plane using 2D LiDAR measurements. Hybrid sensor SLAM in featureless environments is presented in [16]. Regarding relative distance and surface tracking, comparable research includes [17] where indoor wall-tracking method is proposed. Work done in [18] introduces a wall-following algorithm combined with artificial potential fields for the purposes of path planning.

The proposed system is designed under the assumptions that a) the operator is able to manually position the UAV in front of the wind-turbine blade; b) there are no multiple surfaces visible inside the UAV's field of view; c) blade's leading edge is placed vertically wrt. the ground.

Contributions of this paper are threefold: introduction of a LiDAR-based wind-turbine blade inspection controller for use in featureless environments; definition of a state diagram of the proposed UAV system that changes modes of operation in stable manner; showcase the feasibility of this method by presenting simulation results along with a real-world inspection scenario performed on a full-scale wind-turbine blade.

This paper is organized as follows. In section II a mathematical model is briefly presented following the feedback term extraction methods used during the inspection. Section III presents the controller structure along with its corresponding state-diagram. Simulation results conducted in Gazebo environment are displayed in section IV, while the experiment results for a full-scale wind-turbine blade inspection scenario are shown in section V. Finally, a short summary along with conclusions is given in section VI.

II. MODELING PRELIMINARIES

In the first part of this section a brief overview of a general UAV mathematical model is given, followed by an explanation of methods for obtaining additional feedback terms using a LiDAR sensor.

A. MATHEMATICAL UAV MODEL

The UAV model is previously studied in various forms from standard quadrotor [19] to variants with movable center of gravity [20]. A brief introduction to the standard quadrotor UAV model is given in this paper.

In order to properly establish a mathematical model, an inertial reference frame $\{e_1, e_2, e_3\}$ and a UAV body-fixed frame $\{b_1, b_2, b_3\}$ need to be introduced. Rotations around the body-fixed frame are represented with Euler angles roll, pitch and yaw (Φ, Θ, Ψ) using Z-Y-X convention. In this paper a standard quadrotor UAV type is considered. The model used for describing UAV dynamics is given as follows:

$$m\ddot{x} + mge_3 = fb_3 \tag{1}$$

$$\mathrm{J}\dot{\boldsymbol{\Omega}} + \boldsymbol{\Omega} \times \mathrm{J}\boldsymbol{\Omega} = M, \tag{2}$$

where the following terms are defined as:

- $x \in \mathbb{R}^3$ - Position of the body-fixed frame w.r.t. the inertial frame,
- $\boldsymbol{\Omega} \in \mathbb{R}^3$ - Angular velocity of the body-fixed frame,
- $\mathrm{J} \in \mathbb{R}^{3\times3}$ - Moment of inertia matrix w.r.t. the body-fixed frame,
- $M \in \mathbb{R}^3$ - Control moment vector acting in the body-fixed frame.
- $f \in \mathbb{R}$ - Control thrust magnitude

Rotor velocities ω_i and system control inputs $(f, \mathbf{M})$ are related using the well known control allocation matrix for cross configuration quadrotors.

B. FEEDBACK MEASUREMENTS

Inspection mode controller, apart from standard sensor measurements such as IMU and GPS, additionally requires several other feedback values to be made available for the duration of inspection. As can be seen in the flowchart depicted in Fig. 3, point cloud analysis results contain following additional feedback terms: distance from the detected plane to the UAV; plane centroid point; plane normal vector.

Measured distance values from point $p = \left[p_x, p_y, p_z\right]^T$ are computed using the obtained plane parameters $Ax+By+Cz+D = 0$ as follows:

$$d_{mv} = \frac{|Ap_x + Bp_y + Cz + D|}{\sqrt{A^2 + B^2 + C^2 + D^2}} \tag{3}$$

To increase robustness against curved surfaces, the detected plane is orthogonally projected to the $b_2 - b_3$ plane around its centroid point. This ensures removal of the plane slope resulting in more consistent distance measurements.

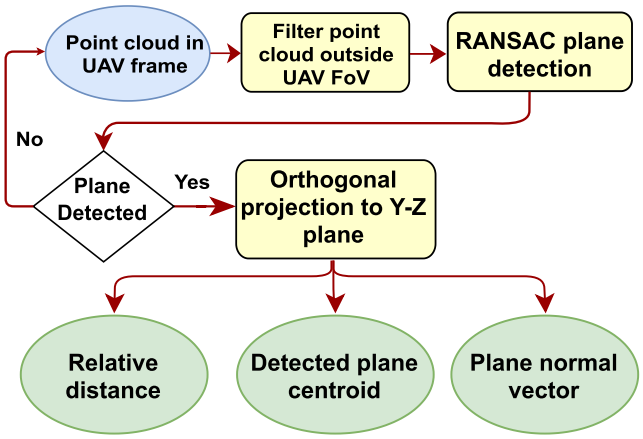

FIGURE 3. Flowchart illustrating point cloud analysis steps used for extracting feedback measurements. Homogeneous transformation is performed on point cloud data obtained from the LiDAR sensor in order to represent it in the UAV frame of reference. In order to speed up the detection process, points outside of the UAV's predetermined field of view (FoV) are filtered out FoV is defined as a point cloud box filter with the UAV's body-fixed frame in its center with the goal of minimizing the number of points going into the detection pipeline. RANSAC algorithm is performed on the remaining point cloud in order to obtain plane parameters. Finally, if plane detection was successful, inferred plane parameters are orthogonally projected to the $b_2 - b_3$ plane in order to improve distance measurements.

Newly obtained plane equation is presented as follows:

$$\frac{A}{\sqrt{A^2+B^2}}x + \frac{B}{\sqrt{A^2+B^2}}y - \begin{bmatrix} A \\ B \\ C \end{bmatrix} \cdot p_{centroid} = 0, \tag{4}$$

$$p_{centroid} = \frac{1}{|\mathbb{S}|}\sum_{i=0}^{|\mathbb{S}|} p_i, \tag{5}$$

where $\mathbb{S}$ is the set of all inlier points of the detected plane.

C. DISCRETE KALMAN FILTER

Additionally, a Discrete Kalman Filter (DKF) [21] is used to obtain relative distance estimation. It serves two purposes: first is to smooth the original measurement signal; second is to ensure continuity of the inspection. If plane detection would fail for any reason (surface clutter, strong wind gusts etc.) DKF will provide model updates until a predetermined timeout period is reached. This enables the UAV to continue the inspection even if the original relative distance feedback is occasionally interrupted. If the elapsed time does pass, plane detection is deemed as failed and transition happens from inspection to position control mode (see Fig. (4.b)).

In order to implement the Kalman filter an *a priori* distance measurement prediction model needs to be defined. However, since distance measurements are obtained through a highly nonlinear optimization method among other things shown in Fig. 3, an exact model is unattainable. Furthermore, there is no characteristic motion dynamics we can pursue in choosing the model nor prior knowledge about the exact shape of wind-turbine blades. However, estimated distance

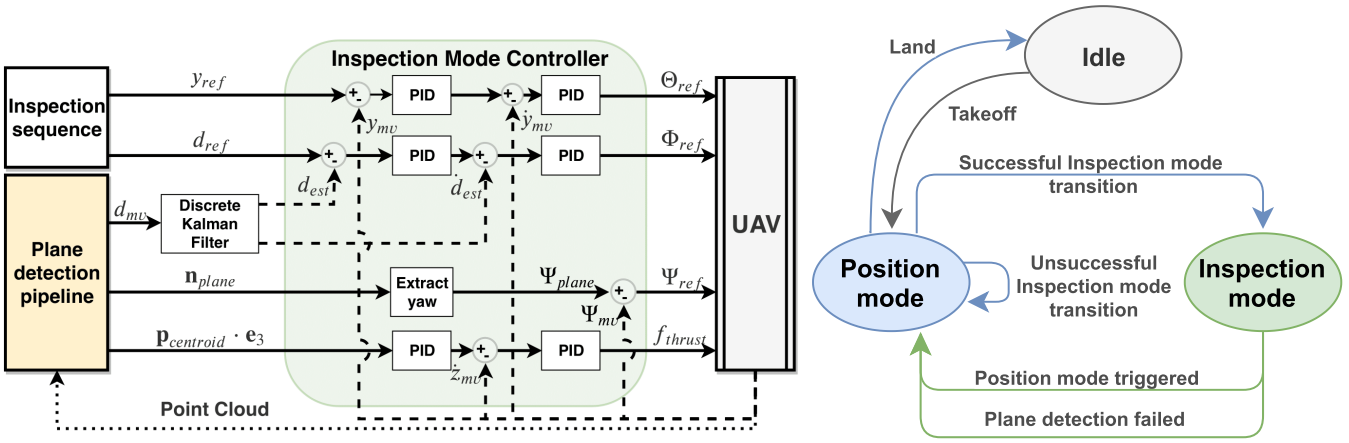

a) The UAV control scheme used when inspection mode is successfully initialized. Position and inspection mode controller structures are identical with main difference being feedback and reference inputs. While the former uses only GPS sensors to determine attitude and thrust targets, the latter utilizes additional feedback and referent values described in II-B.

b) A state machine diagram for the wind-turbine blade inspection hybrid system. Every transition, except *Plane detection failed*, between three presented states is meant to be manually triggered by the designated pilot.

FIGURE 4. A state machine diagram for the wind-turbine blade inspection hybrid system. Every transition, except *Plane detection failed*, between three presented states is meant to be manually triggered by the designated pilot.

is in this case used as a position measurement along the b_1 axis. Therefore, inspired by the UAV dynamics (1) and (2), a constant velocity model is chosen to act as a rigid-body position estimate under the assumption of limited acceleration i.e. pitch angle never exceeds 0.15 *rad*. Model is given as follows:

$$x_{k+1} = \mathrm{F}_k x_k + w_k, \quad \mathrm{F}_k = \begin{bmatrix} 1 & T_s \\ 0 & 1 \end{bmatrix}, \tag{6}$$

where $x_k = \left[d_k,\ \dot{d}_k\right]^T \in \mathbb{R}^2$ is the state vector and $w_k \in \mathbb{R}^2$ acts as process noise for respective states. Observations are made through the following linear system:

$$z_k = \mathrm{H}_x x_k + v_k, \quad \mathrm{H}_k = \begin{bmatrix} 1 & 0 \\ 0 & 0 \end{bmatrix}, \tag{7}$$

where $z_k = [d_{mv},\ 0]^T \in \mathbb{R}^2$ is the obtained state measurement vector and $v_k \in \mathbb{R}^2$ represents the additive noise. Vectors w_k and v_k are considered as independent zero-mean Gaussian distributions with variances Q_i and R_i, $i \in (1, 2)$ respectively. Noise values are determined based on signal-to-noise ratios. Innovation update rule equations are omitted for brevity as they are conventional for DKF.

III. INSPECTION MODE CONTROLLER

First part of this section presents the inspection mode controller structure and how it is integrated in the control loop. State machine diagram for utilization of the inspection mode controller is introduced in the final part with its stability subsequently claimed.

A. CONTROLLER STRUCTURE

First of all, the alternate UAV position expressed in its body fixed frame (b_1, b_3, b_3) obtained by merging GPS and measurements from Section II-B is expressed as follows:

$$x_{local} = d_{est}\, b_1 + y_{\text{gps}}\, b_2 + p_{centroid} \cdot e_3\, b_3, \tag{8}$$

where measurements along b_1 and b_2 are absolute while b_3 is relative. Apart from body velocities, (8) is the main feedback source used by the inspection mode controller.

The control loop structure, presented in Fig. 4.a), mainly consists of cascade PID blocks to determine attitude and thrust targets. Pitch is generated using relative estimated distance and its velocity; roll is determined using position references along b_2 axis and GPS based feedback; yaw is directly computed using the plane normal vector; thrust is produced applying the plane centroid height offset as a PID controller error input. Since the proposed height setpoint value is considered as a relative offset with desired value at zero, an explicit feedback term before z-position PID is not necessary. Attitude control is performed by the onboard flight controller.

It is important to mention the inspection sequence generator block, Fig. (4.a), which is responsible for producing position references along the b_2 body-fixed frame axis which consequently impact the flow of the inspection process as well as setting the initial relative distance reference. Furthermore, it has no additional effect on the switching hybrid system shown in Fig. (4.b), since it operates within the inspection control mode. Lastly, to properly conduct the inspection, UAV needs to traverse to and from the blade tip. The sequence direction switches when the plane inlier points inside UAV's FoV start shrinking in the horizontal direction.

B. STATE MACHINE

As seen in Fig. (4.b) three states are available in the proposed hybrid system. An idle state, during which the UAV is

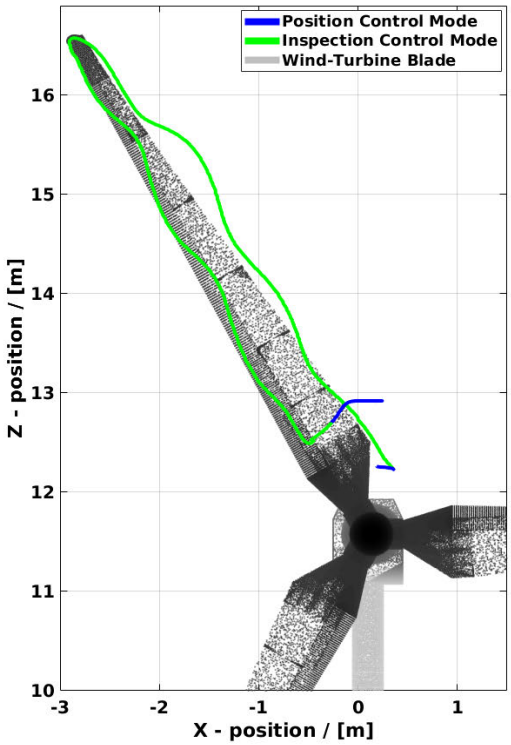

FIGURE 5. This figure shows the local position trajectory during the simulated inspection scenario. Blue and green colored trajectories show pilot-controlled position mode and inspection control mode, respectively. It is important to highlight blade elevation tracking achieved by applying plane centroid offsets as references for the height controller. Ground truth meshes of the wind-turbine blade used in the Gazebo simulation environment is given only as a visual reference.

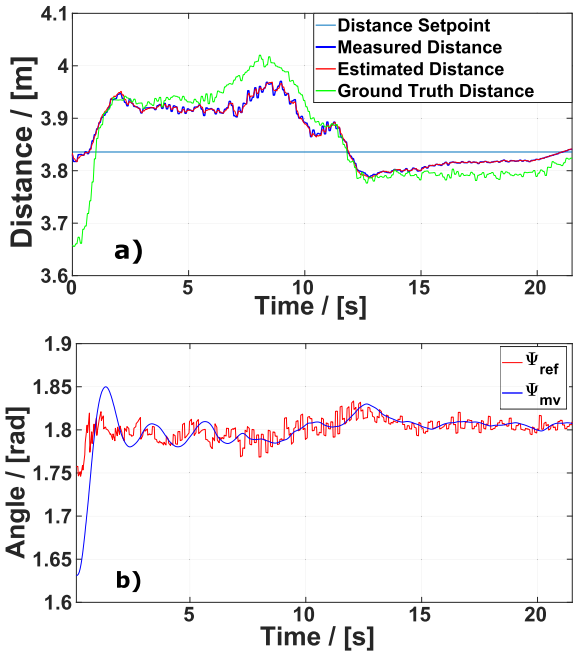

FIGURE 6. Top figure shows a comparison between measured, estimated and ground truth distances during the wind-turbine blade inspection section of the simulation. Distance measurements are computed from the body-fixed frame to the detected plane, while ground truth represents the closest point from the wind-turbine blade mesh to the body-fixed frame. Referent tracking distance is 3.84 *m* set at the start of inspection mode with calculated RMSE at 0.06. Bottom figure shows referent and measured values for yaw angle w.r.t. the body-fixed frame.

grounded. Position control mode is activated after the UAV takes off. This mode uses a standard PID cascade controller structure whose referent position values are issued by the pilot, while GPS sensor supplies high-frequency feedback information. Inspection mode controller, while similar in structure to the previous one, is manually activated when the UAV is near a wind-turbine blade. If transition is successful the UAV adopts a control loop presented in Fig. 4.a). Apart from GPS, additional LiDAR-supplied feedback and referent values are utilized.

The three proposed states assume the following linear system:

$$\dot{\boldsymbol{\zeta}}(t) = \mathrm{A}(t)\boldsymbol{\zeta}(t), \quad \mathrm{A}(t) \in \{\mathrm{A}_1, \mathrm{A}_2, \mathrm{A}_3\}, \tag{9}$$

together forming a switching system. Linear controllers ensure that transition matrices A_2 and A_3, corresponding to position and inspection control modes respectively, are stable with respect to the Hurwitz criterion. Matrix A_1 representing the Idle state is not considered due to its static behavior - UAV is on the ground.

Similar dynamics can be observed from both inspection and position control modes, since only feedback and referent values differ. It is, then, straightforward to show that matrices A_2 and A_3 commute, i.e. $[\mathrm{A}_2,\ \mathrm{A}_3] = \mathrm{A}_2\mathrm{A}_3 - \mathrm{A}_3\mathrm{A}_2 = 0$.

Therefore, according to Theorem I. in [22], there exists a common Lyapunov function of the form $V(\boldsymbol{\zeta}) = \boldsymbol{\zeta}^T \mathrm{P} \boldsymbol{\zeta}$ with a negative definite time-derivative for each state in (9) which guarantees exponential system stability for an arbitrary switching sequence.

IV. SIMULATION RESULTS

Simulations are performed in the Gazebo environment using Robot Operating System (ROS). Flight controller functionalities such as attitude and thrust control available on the experimental UAV setup, described in section V, are simulated using the Software-In-The-Loop method (SITL). Identical firmware running on the onboard flight controller is attached to the UAV used in the simulation. This enables smoother transitions between the hardware and the software, with minimal additional parameter tuning and no code adjustments.

In order to complete the experiment, a full scale wind-turbine blade and rotor model was added to the simulation environment. Inspection is performed on the blade at a 60° angle to also showcase altitude adjustments as well as distance tracking and constant heading. Simulation results are presented in Fig. 5 and 6.

V. EXPERIMENTAL RESULTS

Experiments are performed using a custom-built UAV equipped with a Velodyne VLP-16 LiDAR sensor shown in 7. Pixhawk is used as an onboard flight controller

FIGURE 7. A custom-built LiDAR-equipped UAV used for performing wind-turbine blade inspection tasks.

running Ardupilot firmware while the offboard control and communication is done through the Intel NUC and ROS integration. The experiment was performed at a wind-turbine farm near Split, Croatia on a horizontally placed, full-scale wind-turbine blade.

After taking off and entering position control mode, pilot triggered the inspection mode in which the UAV performed the green colored trajectory shown in Fig. 8. Autonomously following the blade surface to its tip and back, the UAV tracked relative distance to the blade as presented in Fig. 9 while continuously keeping its heading perpendicular to the blade. During the experiment camera and LiDAR data was collected in order to show the feasibility of this inspection method. High-resolution in-focus photographs of blade segments and even a 3D wind-turbine blade model shown in Fig. 8 can be consequently obtained.

TABLE 1. RMSE values for experimental results with a small-scale mock-up and a full-scale wind-turbine blade. Tracking and detection errors are calculated as a difference between distance setpoint versus measurements and inferred plane points versus surrounding pointcloud respectively.

Setup	Distance Tracking [m]	Detection Error [m]
Mock-up blade	0.1807	0.1272
Mock-up blade	0.1256	0.1238
Mock-up blade	0.1429	0.1315
Mock-up blade	0.1439	0.1284
Mock-up blade	0.1759	0.1173
Mock-up blade	0.2066	0.1199
Mock-up blade	0.1748	0.1161
Turbine blade	0.2885	0.1167
Turbine blade	0.1916	0.0877

Furthermore, prior to conducting the field tests, multiple preliminary experiments on a wall as well as a wind-turbine blade mock-up setup were performed. To further support our claim we present the results of inspections conducted on an experimental mock-up setup and a full-scale wind-turbine blade in Table 1. The mock-up blade was designed as a white, non curved surface, 8m long and 1.5m wide, hung at 3m from the ground. Results are presented as distance tracking and plane detection RMSE values in order to showcase the system's performance. Video playlist of the field experiments

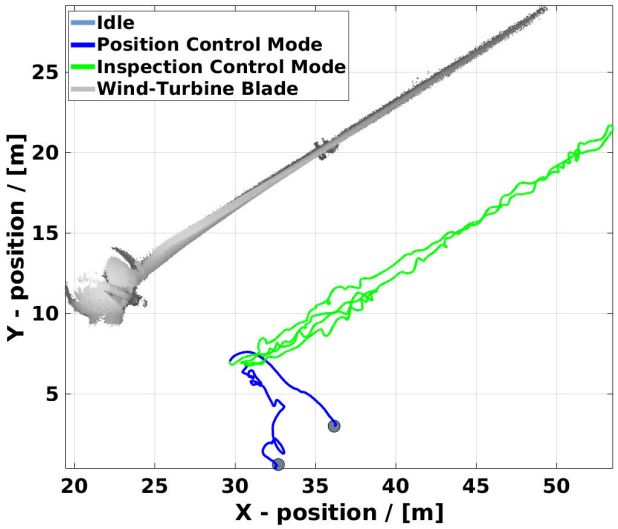

FIGURE 8. This figure shows the local position trajectory during the experimental wind-turbine blade inspection scenario obtained from GPS measurements. Blue and green colored trajectories show the pilot-controlled position mode and autonomous inspection control mode respectively. Slate gray colored markers represent takeoff and landing positions. The wind-turbine blade model obtained post-inspection is shown only as a visual reference.

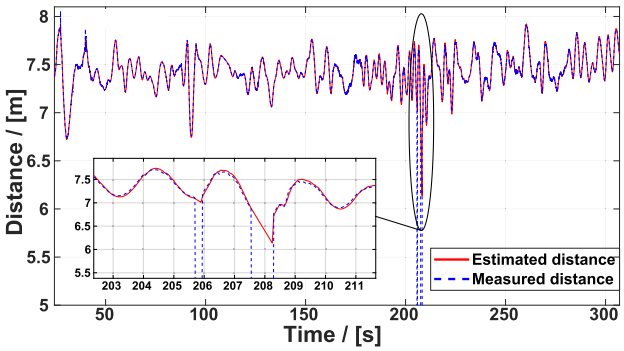

FIGURE 9. A comparison between measured and estimated distances during the wind-turbine blade inspection section of the experiment. Referent tracking distance is 7.38 *m* set at the start of inspection mode with calculated RMSE at 0.1916 *m*. Outlined section of the plot depicts two instances where distance measurements were nonexistent due to the lack of detectable surfaces. It can be seen that during such occurrences estimated distance is able to compensate for the loss of measurements and inspection remains uninterrupted.

with full scale and mock-up wind-turbine blades can be found in [23].

VI. CONCLUSION AND FUTURE WORK

In this paper, an autonomous wind-turbine blade inspection procedure using LiDAR-equipped UAV is presented. Designed specifically for use in featureless off-shore environments, with no additional pre-flight setup required, such as trajectory generation and prior wind-turbine structure knowledge. The inspection mode controller was introduced and implemented within a state machine framework with the underlying hybrid switching system proven exponentially

stable. Feasibility of this procedure is affirmed by simulation results, and experimentally on a mock-up blade and a full-scale wind-turbine blade.

The idea for future work is to expand the existing inspection framework to accommodate a variety of target structures such as bridges, high-voltage lines, buildings etc. Issues of robustness, due to unfavorable conditions at wind-turbine farms, can be addressed in further research by enhancing the Inspection Controller with a Hsia structure as presented in [24]. Furthermore, we will investigate the issue of moving blade inspections as well as projecting image data on the obtained 3D model as a part of the post processing analysis.

REFERENCES

[1] *Aerotwin Project*. Accessed: Sep. 10, 2019. [Online]. Available: https://aerotwin.fer.hr/
[2] *Encore Project*. Accessed: Sep. 10, 2010. [Online]. Available: http://encorebim.eu/, accessed: 2019-09-10.
[3] R. Mattar and R. Kalai, "Development of a wall-sticking drone for non-destructive ultrasonic and corrosion testing," *Drones*, vol. 2, no. 1, p. 8, Feb. 2018, doi: 10.3390/drones2010008.
[4] K. Máthé and L. Buşoniu, "Vision and control for UAVs: A survey of general methods and of inexpensive platforms for infrastructure inspection," *Sensors*, vol. 15, no. 7, pp. 14887–14916, Jun. 2015, doi: 10.3390/s150714887.
[5] A. Ollero, J. Cortes, A. Santamaria-Navarro, M. A. T. Soto, R. Balachandran, J. Andrade-Cetto, A. Rodriguez, G. Heredia, A. Franchi, G. Antonelli, K. Kondak, A. Sanfeliu, A. Viguria, J. R. Martinez-de Dios, and F. Pierri, "The AEROARMS project: Aerial robots with advanced manipulation capabilities for inspection and maintenance," *IEEE Robot. Autom. Mag.*, vol. 25, no. 4, pp. 12–23, Dec. 2018, doi: 10.1109/mra.2018.2852789.
[6] J. Sun, B. Li, Y. Jiang, and C.-Y. Wen, "A camera-based target detection and positioning UAV system for search and rescue (SAR) purposes," *Sensors*, vol. 16, no. 11, p. 1778, Oct. 2016, doi: 10.3390/s16111778.
[7] D. Roca, J. Armesto, S. Lagüela, and L. Díaz-Vilariño, "Lidar-equipped UAV for building information modelling," *ISPRS-Int. Arch. Photogramm., Remote Sens. Spatial Inf. Sci.*, vols. XL–5, pp. 523–527, Jun. 2014.
[8] C. Kanellakis, E. Fresk, S. S. Mansouri, D. Kominiak, and G. Nikolakopoulos, "Autonomous visual inspection of large-scale infrastructures using aerial robots," 2019, *arXiv:1901.05510*. [Online]. Available: http://arxiv.org/abs/1901.05510
[9] O. Moolan-Feroze, K. Karachalios, D. N. Nikolaidis, and A. Calway, "Simultaneous drone localisation and wind turbine model fitting during autonomous surface inspection," 2019, *arXiv:1904.04523*. [Online]. Available: http://arxiv.org/abs/1904.04523
[10] M. Stokkeland, K. Klausen, and T. A. Johansen, "Autonomous visual navigation of unmanned aerial vehicle for wind turbine inspection," in *Proc. Int. Conf. Unmanned Aircr. Syst. (ICUAS)*, Jun. 2015, pp. 998–1007, doi: 10.1109/icuas.2015.7152389.
[11] C. L. Glennie, A. Kusari, and A. Facchin, "Calibration and stability analysis of the VLP-16 laser scanner," *ISPRS-Int. Arch. Photogramm., Remote Sens. Spatial Inf. Sci.*, vols. XL–3/W4, pp. 55–60, Mar. 2016, doi: 10.5194/isprsarchives-xl-3-w4-55-2016.
[12] G. Morgenthal and N. Hallermann, "Quality assessment of unmanned aerial vehicle (UAV) based visual inspection of structures," *Adv. Struct. Eng.*, vol. 17, no. 3, pp. 289–302, Mar. 2014, doi: 10.1260/1369-4332.17.3.289.
[13] M. Yadav, B. Lohani, and A. K. Singh, "Road surface detection from mobile LiDAR data," *ISPRS Ann. Photogramm., Remote Sens. Spatial Inf. Sci.*, vol. IV-5, pp. 95–101, 2018. [Online]. Available: https://doi.org/10.5194/isprs-annals-iv-5-95-2018, doi: 10.5194/isprs-annals-iv-5-95-2018.
[14] K. Miadlicki, M. Pajor, and M. Saków, "Ground plane estimation from sparse LIDAR data for loader crane sensor fusion system," in *Proc. 22nd Int. Conf. Methods Models Autom. Robot. (MMAR)*, Aug. 2017, pp. 717–722, doi: 10.1109/mmar.2017.8046916.
[15] C. Berger, "Toward rich geometric map for SLAM : Online detection of planes in 2D LIDAR," *J. Automat. Mobile Robot. Intell. Syst.*, vol. 7, no. 1, pp. 35–41, 2013.
[16] T. Oh, H. Kim, K. Jung, and H. Myung, "Graph-based SLAM approach for environments with laser scan ambiguity," in *Proc. 12th Int. Conf. Ubiquitous Robots Ambient Intell. (URAI)*, Oct. 2015, pp. 139–141.
[17] A. Nemati, M. Sarim, M. Hashemi, and M. Kumar, "Autonomous wall-following based navigation of unmanned aerial vehicles in indoor environments," in *AIAA Infotech Aerospace*. Reston, VI, USA: American Institute of Aeronautics and Astronautics, Jan. 2015, doi: 10.2514/6.2015-0989.
[18] H. Wang, M. Cao, H. Jiang, and L. Xie, "Feasible computationally efficient path planning for UAV collision avoidance," in *Proc. IEEE 14th Int. Conf. Control Autom. (ICCA)*, Jun. 2018, pp. 576–581, doi: 10.1109/icca.2018.8444284.
[19] D. Mellinger and V. Kumar, "Minimum snap trajectory generation and control for quadrotors," in *Proc. IEEE Int. Conf. Robot. Autom.*, May 2011, pp. 2520–2525, doi: 10.1109/icra.2011.5980409.
[20] L. Markovic, A. Ivanovic, M. Car, M. Orsag, and S. Bogdan, "Geometric tracking control of aerial robots based on centroid vectoring," in *Proc. 18th Eur. Control Conf. (ECC)*, Jun. 2019, pp. 2701–2706, doi: 10.23919/ecc.2019.8795829.
[21] C. K. Chui and G. Chen, *Kalman Filtering With Real-Time Applications*. Berlin, Germany: Springer-Verlag, 1987.
[22] K. S. Narendra and J. Balakrishnan, "A common Lyapunov function for stable LTI systems with commuting A-matrices," *IEEE Trans. Autom. Control*, vol. 39, no. 12, pp. 2469–2471, Dec. 1994, doi: 10.1109/9.362846.
[23] M. Car, L. Markovic, A. Ivanovic, M. Orsag, and S. Bogdan. (Sep. 2019). *Wind-Turbine Blade Inspection*. [Online]. Available: https://www.youtube.com/playlist?list=PLC0C6uwoEQ8a1pqgPeBR3N927XOjLm8XU
[24] M. Orsag, T. Haus, I. Palunko, and S. Bogdan, "State estimation, robust control and obstacle avoidance for multicopter in cluttered environments: EuRoC experience and results," in *Proc. Int. Conf. Unmanned Aircr. Syst. (ICUAS)*, Jun. 2015, pp. 455–461.

MARKO CAR (Member, IEEE) received the B.S.E.E. and M.S.E.E. degrees from the University of Zagreb, Croatia, in 2013 and 2015, respectively, where he is currently pursuing the Ph.D. degree.

He is employed as a Research Associate at the Faculty of Electrical Engineering and Computing, University of Zagreb. His main research interests include aerial robotics, control theory, and autonomous systems. In his undergraduate years, he received the University of Zagreb Rector Award for the Best Student Projects, in 2014.

LOVRO MARKOVIC (Member, IEEE) received the B.S.E.E. and M.S.E.E. degrees from the University of Zagreb, Croatia, in 2016 and 2018, respectively, where he is currently pursuing the Ph.D. degree.

He is employed as a Research Associate at the Faculty of Electrical Engineering and Computing, University of Zagreb. His latest publication includes *Geometric Tracking Control of Aerial Robots Based on Centroid Vectoring*. His main research interests include aerial robotics, geometric control theory, and autonomous operation systems.

ANTUN IVANOVIC (Member, IEEE) received the B.S.E.E. and M.S.E.E. degrees from the University of Zagreb, Croatia, in 2013 and 2015, respectively, where he is currently pursuing the Ph.D. degree.

He is employed as a Research Associate at the Faculty of Electrical Engineering and Computing, University of Zagreb. His main research interests include aerial robotics, motion planning, and autonomous systems. In his undergraduate years, he received the University of Zagreb Rector Award for the Best Student Projects, in 2014.

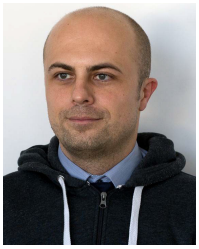

MATKO ORSAG (Member, IEEE) received the B.S.E.E., M.S.E.E., and Ph.D. degrees from the University of Zagreb (UNIZG), Croatia, in 2008, 2010, and 2015, respectively.

As a Researcher, he has participated in several national and international research projects in the field of robotics, control, and automation. From 2011 to 2012, he worked as a Visiting Researcher at Drexel University, Philadelphia, PA, USA. He is currently an Assistant Professor with the Faculty of Electrical Engineering and Computing (FER), UNIZG. He has authored or coauthored over 30 scientific and professional papers, including journal articles and conference papers, and a monograph and a book chapter in the field of unmanned aerial systems and robotics. His main research interests include autonomous systems, robotics, and intelligent control systems. He was a recipient of the Fulbright Exchange Grant.

STJEPAN BOGDAN (Senior Member, IEEE) received the B.S.E.E. and M.S.E.E. degrees and the Ph.D. degree in EE from the University of Zagreb (UNIZG), Croatia, in 1990, 1993, and 1999, respectively.

He is currently a Full Professor with the Laboratory for Robotics and Intelligent Control Systems (LARICS), Department on Control and Computer Engineering, Faculty of Electrical Engineering and Computing (FER), UNIZG. He spent one year as a Fulbright Researcher at the Automation and Robotics Research Institute, Arlington, USA, in Prof. Frank Lewis' Lab. He is the coauthor of four books and numerous articles published in journals and proceedings. His main research interests include autonomous systems, aerial robotics, multiagent systems, intelligent control systems, bio-inspired systems, and discrete event systems.